ELSEVIER

Journal of Power Sources 75 (1998) 1–8

JOURNAL OF POWER SOURCES

Corrosion behaviour of $Zr_{1-x}Ti_xV_{0.6}Ni_{1.2}M_{0.2}$ (M = Ni, Cr, Mn) AB_2-type metal hydride alloys in alkaline solution

J.S. Kim [a,1], C.H. Paik [a,*], W.I. Cho [a], B.W. Cho [a], K.S. Yun [a], S.J. Kim [b]

[a] *Korea Institute of Science and Technology, Seoul, South Korea*
[b] *Seoul National University, Seoul, South Korea*

Received 13 February 1998; accepted 26 February 1998

Abstract

An examination is made of the discharge and cycle life of $Zr_{0.5}Ti_{0.5}V_{0.6}Ni_{1.4}$ alloys when a fraction (0.2 at.%) of the Ni-component is substituted by Cr or Mn. In addition, the Zr:Ti component ratios are varied to extend the cycle life of high capacity, Mn-substituted $Zr_{1-x}Ti_xV_{0.6}Ni_{1.2}Mn_{0.2}$ ($x = 0.0$, 0.25, 0.5, 0.75) alloys. The metallurgical microstructure is observed by X-ray diffraction analysis, scanning electron microscopy, and energy dispersive X-ray analysis. Active–passive potentiodynamic behaviour, as well as charge–discharge cycle characteristics, is evaluated, and dissolved V-species in the electrolytic solution is analyzed by inductively coupled plasma spectroscopy. The corrosion behaviour of the V–Cr or the V–Mn phase in the alkaline electrolyte solution is found to determine the cycle life of an AB_2 alloy. Cr-substituted ($Zr_{0.5}Ti_{0.5}Ni_{1.2}Cr_{0.2}$) alloy, containing a V–Cr phase, is estimated to involve a dissolution rate of 0.028 wt.% vanadium per cycle in an alkaline electrolytic solution, while Mn-substituted ($Zr_{0.5}Ti_{0.5}V_{0.6}Ni_{1.2}Mn_{0.2}$) alloy, containing a V–Mn phase, is estimated to have a dissolution rate of 0.138 wt.% vanadium per cycle. For Mn-substituted alloys, an optimum Zr:Ti ratio of 3:1, i.e., $Zr_{0.75}Ti_{0.25}V_{0.6}Ni_{1.2}Mn_{0.2}$, is found to have the most stable cycle life. The improvement in cycle life caused by increasing the Zr content in the alloy is attributed to increase in the corrosion resistance of the alloy due to less formation of the corrosive V–Mn phase.

Keywords: AB_2-type metal hydride; Vanadium solid solution; Electrode cycle life; Vanadium dissolution

1. Introduction

A gradual decrease in the hydrogen-storage capacity of the metal hydride (MH) electrode during repeated cycling is attributed to deterioration of the alloy powder [1] and dissolution of the constituent species [2,3]. For AB_2 alloys, previous studies have shown that the manganese-containing alloy ($Zr_{0.5}Ti_{0.5}V_{0.6}Ni_{1.2}Mn_{0.2}$) electrode exhibits a particularly high discharge capacity, but a rather short cycle life. The chromium-containing alloy ($Zr_{0.5}Ti_{0.5}Ni_{1.2}Cr_{0.2}$) electrode, on the other hand, maintains a more stable cycle performance despite its initially lower capacity [4,5]. In this paper, an attempt is made to improve the cycle life of manganese-containing alloy electrodes while maintaining their inherent high discharge capacity.

Preferential dissolution of vanadium in the alloy is known to be a major factor in corrosion of the above alloys in alkaline electrolyte solutions [2]. The V–Cr phase can stabilize the passive film while the V–Mn phase suffers higher dissolution [5]. Since vanadium can also form a solid solution with titanium [6], it can be expected that the amount of V–Mn phase, shown to be susceptible to vanadium dissolution, could be influenced by lowering the titanium content in the alloy.

In this work, the electrochemical characteristics of Zr-Ti-V-Ni-M alloys with variations in both the metal components M = Ni, Mn, Cr and the Zr:Ti ratios are investigated in terms of discharge capacity, cycle life, and corrosion behaviour. The dissolution rate of the vanadium species has been monitored by both the potentiodynamic behaviour [7] and the resulting analysis of the vanadium ions in the electrolytic solution.

* Corresponding author.
[1] Current address: Hanil Valence, Co. Ltd., Seoul, Korea.

0378-7753/98/$19.00
PII S0378-7753(98)00075-5

2. Experimental apparatus and procedure

Two series of hydrogen-storage alloys were prepared by arc melting in an argon atmosphere, namely, $Zr_{0.5}Ti_{0.5}V_{0.6}Ni_{1.2}M_{0.2}$ (M = Ni, Cr, Mn) and $Zr_{1-x}Ti_xV_{0.6}Ni_{1.2}Mn_{0.2}$ (x = 0.0, 0.25, 0.5, 0.75). In order to study the microstructure of the alloys, each ingot was polished, etched, and examined by scanning electron microscopy (SEM, Hitachi S-250). Compositions of the different phases in the alloy were determined by energy dispersive X-ray microanalysis (EDX, JEOL JXA-8600). The crystal structures of the alloys were identified by powder X-ray diffraction (XRD, Rigaku) analysis with Cu Kα radiation. Potentiodynamic polarization was measured by means of a solartron SI 1286 Electrochemical Interface to evaluate the corrosion behaviour of the alloy ingots.

For charge–discharge testing, the alloy ingots were pulverized into powder by a single-cycle process of hydrogen absorption and desorption in a pressure vessel followed by sieving to under 200 mesh (< 75 μm). The alloy powder (0.4 g) was thoroughly mixed with teflonized acetylene black (0.8 g, IBA TAB-3), and its mixture (2 cm diameter) was pressed between two foamed nickel plates (Eltech). The MH electrode was wrapped with polyamide separator and sandwiched between two pasted nickel hydroxide electrodes. The resulting electrodes were fixed between two Plexiglas plates by means of stainless-steel bolts and then tested in an MH electrode-limited half cell. The reference electrode was a Hg/HgO electrode; all potentials are reported with respect to this electrode. The electrolytic solution consisted of 30 wt.% KOH solution with 1 M LiOH. The MH electrode was charged with a

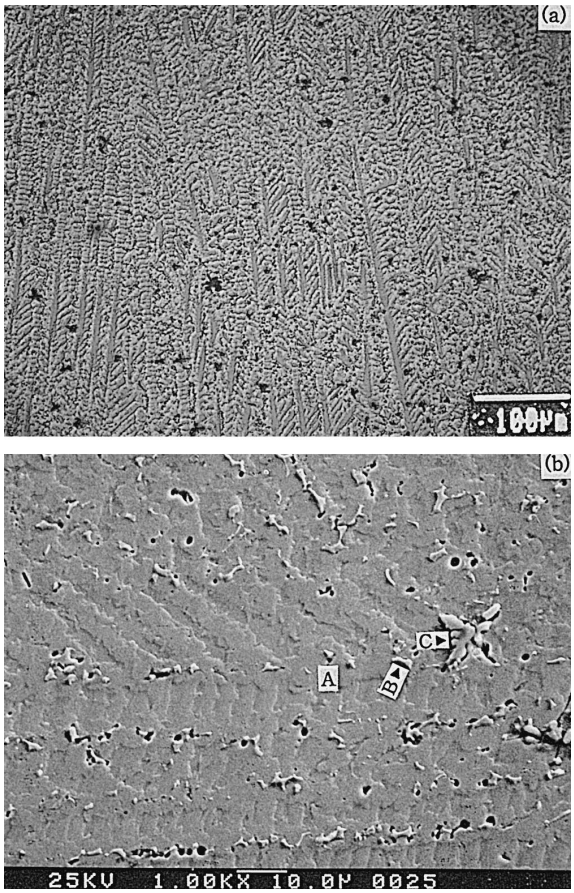

Fig. 2. (a) Optical micrograph and (b) scanning electron micrograph of $Zr_{0.5}Ti_{0.5}V_{0.6}Ni_{1.4}$.

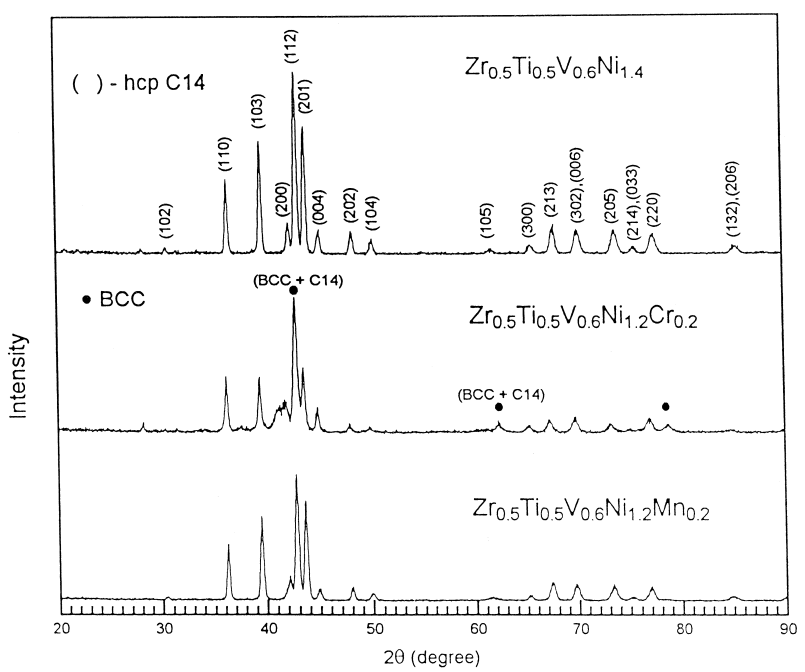

Fig. 1. X-ray diffraction patterns of $Zr_{0.5}Ti_{0.5}V_{0.6}Ni_{1.2}M_{0.2}$ (M = Ni, Cr, Mn) alloy powders.

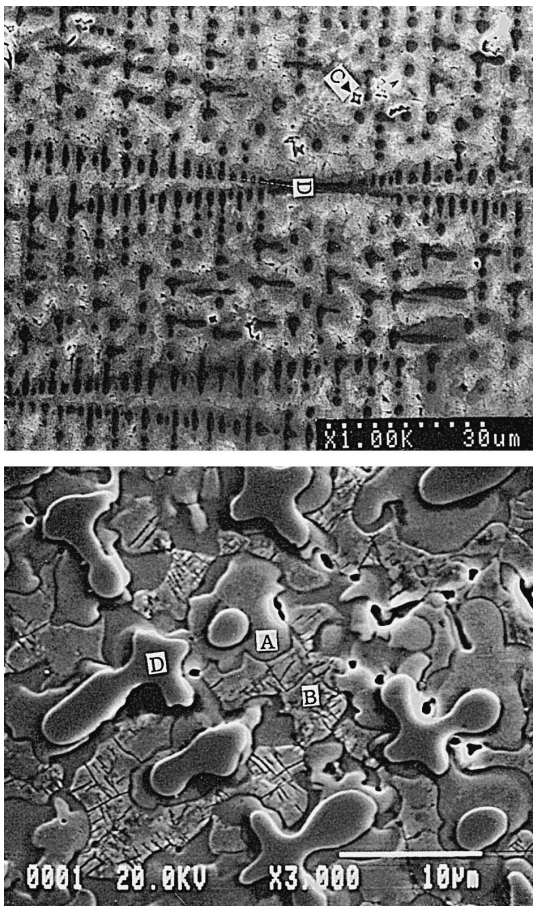

Fig. 3. Scanning electron micrographs of $Zr_{0.5}Ti_{0.5}V_{0.6}Ni_{1.2}Cr_{0.2}$.

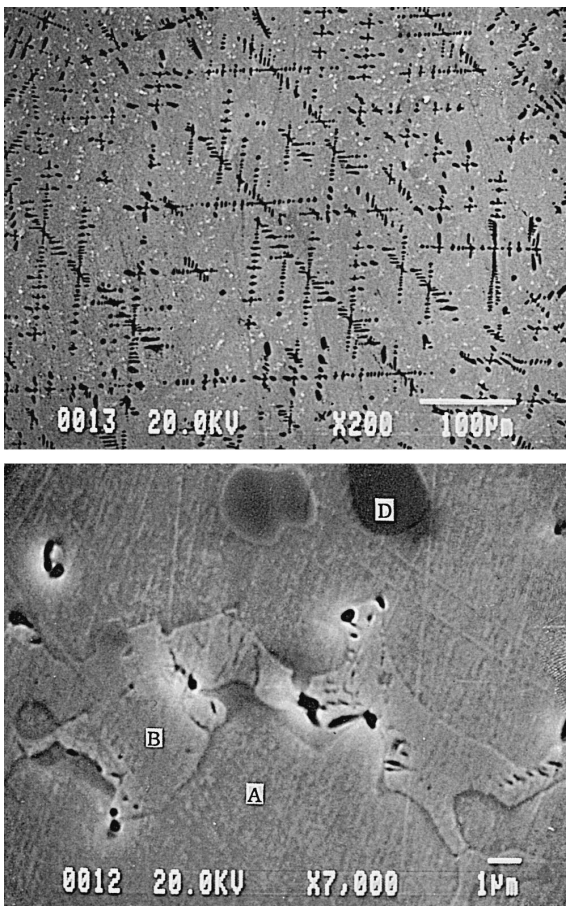

Fig. 4. Scanning electron micrographs of $Zr_{0.5}Ti_{0.5}V_{0.6}Ni_{1.2}Mn_{0.2}$.

constant current density of 60 mA g^{-1} for 400–480 min and discharged to −0.7 V (vs. Hg/HgO) with the same current density, both at room temperature.

Cycle testing was performed by a d.c. power supply (Jisang, JEC-16, 1 A) interfaced to an IBM compatible PC A/D converter. After the cycle life testing, the electrolyte solutions were analyzed by inductively coupled plasma spectroscopy (ICP, Thermo Jarrell Ash PolyScan 61E) and

Table 1
EDX analysis (at.%) of composition of $Zr_{0.5}V_{0.5}V_{0.6}Ni_{1.2}M_{0.2}$ alloys (M = Ni, Cr, Mn)

		M = Ni	M = Cr	M = Mn			M = Ni	M = Cr	M = Mn
Wide-area scanning	Zr	16.5	16.6	16.1					
	Ti	16.1	16.0	17.1					
	V	22.8	23.3	22.2					
	Ni	44.5	36.9	38.7					
	M	–	7.2	5.9					
A (matrix, C14)	Zr	16.2	15.7	16.0	C (Zr-rich)	Zr	94.6	93.0	–
	Ti	15.1	14.9	17.5		Ti	0.7	1.5	–
	V	24.1	17.2	21.9		V	1.1	2.1	–
	Ni	44.5	48.6	38.7		Ni	3.6	3.1	–
	M	–	3.5	5.9		M	–	0.3	–
B (Zr–Ti–Ni)	Zr	10.4	18.2	12.3	D (V-rich)	Zr	–	0.6	0.1
	Ti	24.2	26.6	27.0		Ti	–	3.8	3.8
	V	9.6	4.4	6.0		V	–	62.8	77.5
	Ni	55.8	50.3	52.7		Ni	–	7.3	7.0
	M	–	0.5	2.0		M	–	25.7	11.6

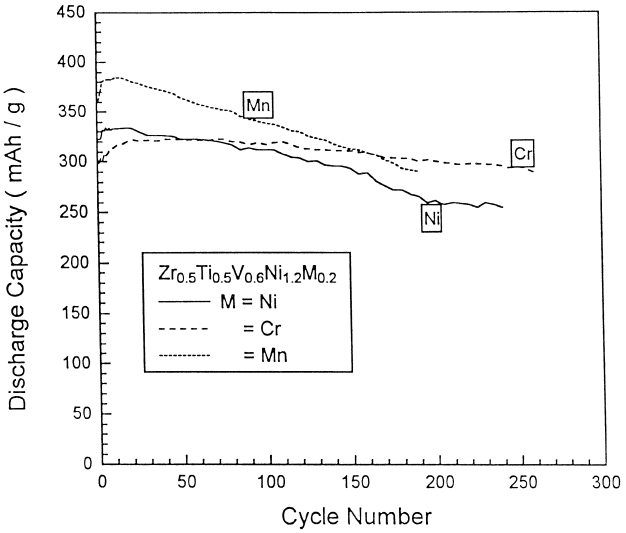

Fig. 5. Cycle performance of $Zr_{0.5}Ti_{0.5}V_{0.6}Ni_{1.2}M_{0.2}$ (M = Ni, Cr, Mn) alloy.

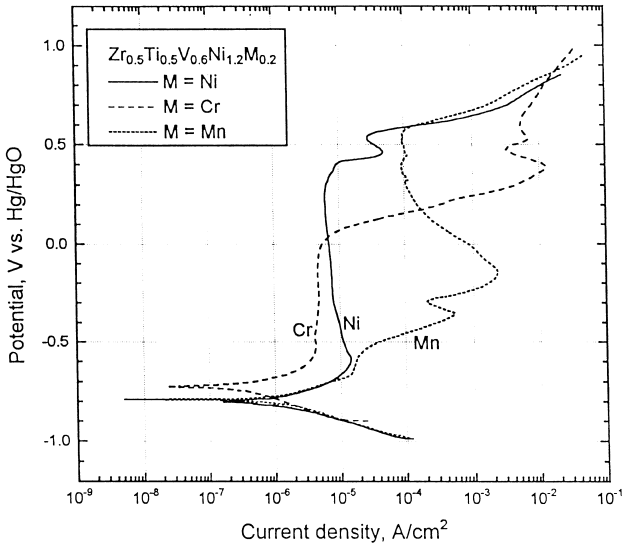

Fig. 6. Potentiodynamic polarization behaviour of $Zr_{0.5}Ti_{0.5}V_{0.6}Ni_{1.2}M_{0.2}$ (M = Ni, Cr, Mn) alloy ingots.

atomic absorption spectroscopy (AAS, Varian SpectrAA-800).

3. Results and discussion

3.1. $Zr_{0.5}Ti_{0.5}V_{0.6}Ni_{1.2}M_{0.2}$ (M = Ni, Cr, Mn) alloy system

3.1.1. Crystal structure and metallurgical microstructure

Fig. 1 shows the X-ray diffraction patterns of $Zr_{0.5}Ti_{0.5}V_{0.6}Ni_{1.2}M_{0.2}$ (M = Ni, Cr, Mn) alloy powders. The main phase of each alloy is a hexagonal C14 Laves phase. The small additional peaks found with the Cr-containing alloys are indexed as a cubic (BCC) structure.

Scanning electron micrographs (SEM) of $Zr_{0.5}Ti_{0.5}V_{0.6}Ni_{1.2}M_{0.2}$ (M = Ni, Cr, Mn) alloys are presented in Figs. 2–4, respectively. The compositional analysis (by means of EDX) was conducted at regions A, B, C, and D; the results are summarized in Table 1. The regions A, B, C, and D are found to be C14 Laves phase, (Zr, Ti)-Ni phase, Zr-rich phase, and V-rich phase, respectively. It is noted that the V-rich phase (D region) is formed by substitution of a small part of the nickel in $Zr_{0.5}Ti_{0.5}V_{0.6}Ni_{1.4}$ alloy with chromium or manganese. The V-rich phases in $Zr_{0.5}Ti_{0.5}V_{0.6}Ni_{1.2}Cr_{0.2}$ and $Zr_{0.5}Ti_{0.5}V_{0.6}Ni_{1.2}Mn_{0.2}$ alloys are found to be V–Cr and V–Mn solid solutions, respectively. From the binary phase diagrams for V–Cr and V–Mn, it can be understood that V forms a BCC solid solution with Cr and Mn over a wide range of composition. Since vanadium metal oxide (VO_x) dissolves in strong alkaline solution and causes the Zr-Ti-V-Ni alloy electrode to have a poor cycle life [2], the

Table 2
Concentration of dissolved vanadium and capacity loss after charge–discharge life tests of $Zr_{0.5}Ti_{0.5}V_{0.6}Ni_{1.2}M_{0.2}$ electrodes (M = Ni, Cr, Mn)

Alloy	Concentration of alloying elements (mg l^{-1})					Dissolved V (%)	Capacity loss (%)	Cycle
	V	Zr	Ti	Ni	M			
M = Ni	80					10.8	12.7	120
M = Cr	25				< 0.2	3.4	2.5	120
M = Cr	75	6.41	0.08	0.24	< 0.2	10.1	16.6	196
M = Mn	178	3.45	0.01	3.19		23.9	24.8	106

Table 3
Corrosion potential (E_{corr}) and current (I_{corr}), percent of capacity decrease and V-dissolution per cycle of $Zr_{0.5}Ti_{0.5}V_{0.6}Ni_{1.2}M_{0.2}$ alloys (M = Ni, Cr, Mn)

M	E_{corr} (V vs. Hg/HgO)	I_{corr} (μA cm^{-2})	Capacity decrease per cycle (%) × 10^2	V-dissolution per cycle (%) × 10^2
Ni	−0.798	1.09	10.6	9.0
Cr	−0.725	0.26	2.1	2.8
Mn	−0.792	1.20	12.8	13.8

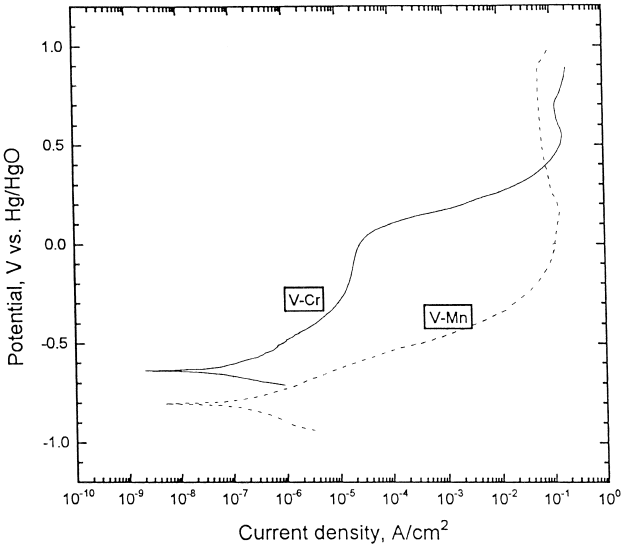

Fig. 7. Potentiodynamic polarization behaviour of V–Cr and V–Mn phases.

corrosion resistance of the vanadium-rich phase present in the alloy can be considered to improve the cycle life of the MH electrode.

3.1.2. Degradation of MH electrode and corrosion behaviour

The cycle performance of $Zr_{0.5}Ti_{0.5}V_{0.6}Ni_{1.2}M_{0.2}$ (M = Ni, Cr, Mn) alloy electrodes is shown in Fig. 5. The Mn-containing alloy exhibited higher capacity but a shorter cycle life than the original $Zr_{0.5}Ti_{0.5}V_{0.6}Ni_{1.4}$ alloy. The Cr-containing alloy gave an increased cycle life. Table 2 lists the amount of dissolved species in the solution (analyzed by ICP) at the end of cycle testing. Vanadium is found to be the most soluble component in the solution, and the rate of capacity decrease is found to be proportional to the rate of vanadium dissolution.

The potentiodynamic behaviour of $Zr_{0.5}Ti_{0.5}V_{0.6}Ni_{1.2}M_{0.2}$ alloy ingots is shown in Fig. 6. A typical MH electrode operates in the potential region −0.6 to −1.0 V. From the rest potential at about −0.8 to −0.7 V, all alloys exhibit a direct passive behaviour when scanned towards more positive potentials. By contrast, the Mn-containing alloy continues to dissolve actively when scanned toward further positive potentials.

Table 3 shows the corrosion potential (E_{corr}) and corrosion current (I_{corr}) of each alloy evaluated from the polarization curves in Fig. 6. The corrosion potential of the Cr-containing alloy is the most positive, with the lowest

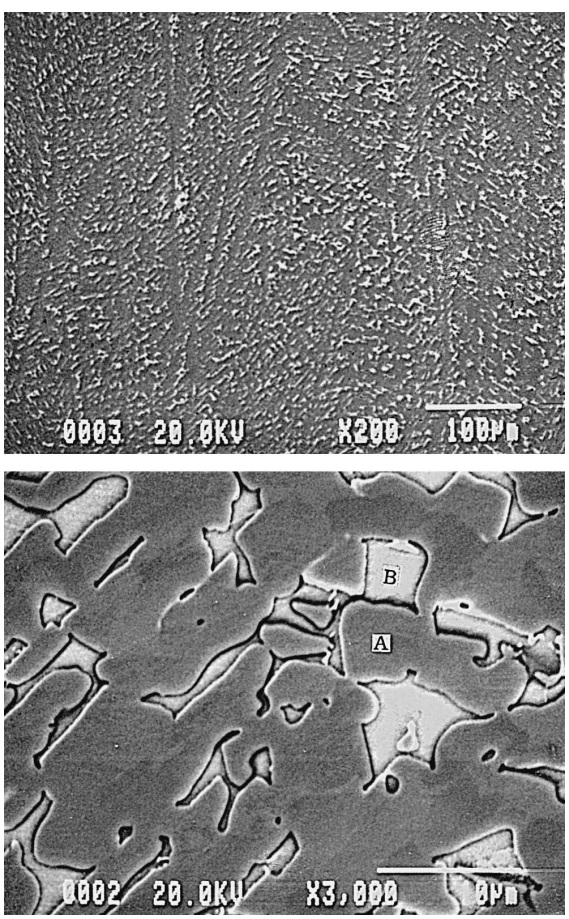

Fig. 8. Scanning electron micrographs of $Zr_{1-x}Ti_xV_{0.6}Ni_{1.2}Mn_{0.2}$ (x = 0.0); magnification: (a) 1000×; (b) 3000×.

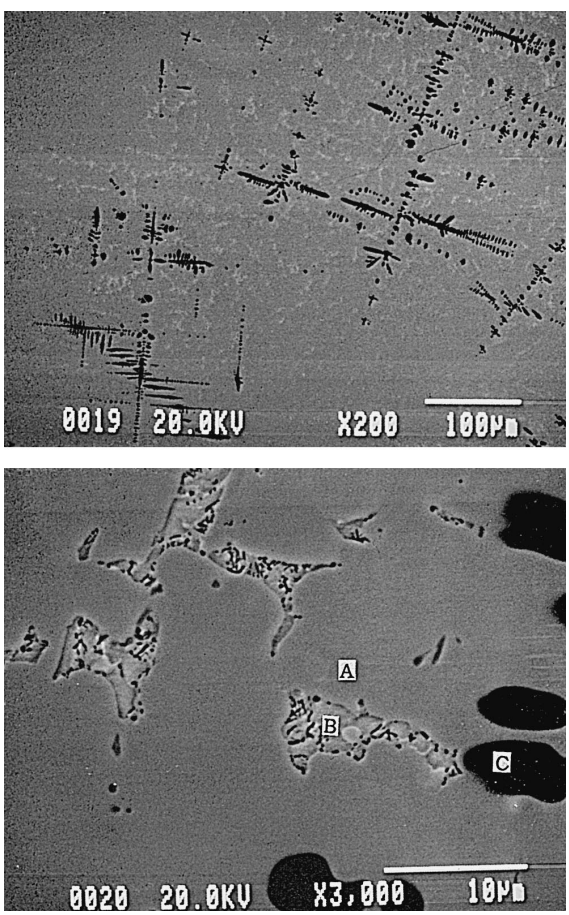

Fig. 9. Scanning electron micrographs of $Zr_{1-x}Ti_xV_{0.6}Ni_{1.2}Mn_{0.2}$ (x = 0.25); magnification: (a) 1000×; (b) 3000×.

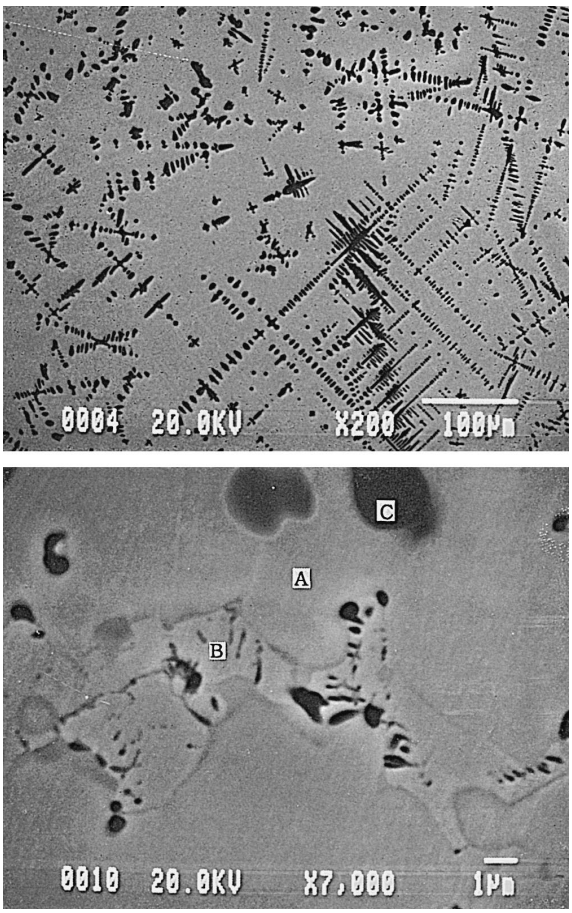

Fig. 10. Scanning electron micrographs of $Zr_{1-x}Ti_xV_{0.6}Ni_{1.2}Mn_{0.2}$ ($x = 0.50$).

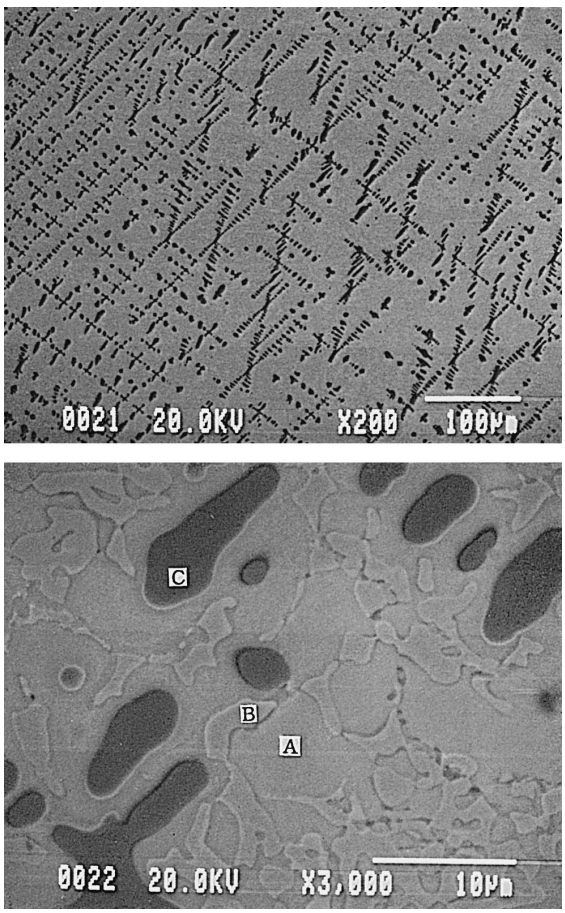

Fig. 11. Scanning electron micrographs of $Zr_{1-x}Ti_xV_{0.6}Ni_{1.2}Mn_{0.2}$ ($x = 0.75$).

current. The stability of the oxide on the Cr-containing alloy, which is apparent above -0.5 V in the polarization curve, is highest amongst all the alloys. In the case of the Mn-containing alloy, both the corrosion potential and the corrosion current are almost the same as the original $Zr_{0.5}Ti_{0.5}V_{0.6}Ni_{1.4}$ alloy, but the stability of the oxide is lower and resulted in a higher dissolution rate of vanadium and, hence, a shorter cycle life.

The difference in the corrosion resistance between Cr- and Mn-containing alloys may be attributed to the difference in the corrosion resistance of the V-rich phase which exists in each alloy. From SEM, EDX, and XRD analysis, it is found that the major components of the V-rich phases in the Cr-containing alloy are V and Cr, while for Mn-containing alloy are V and Mn. It is well known that Cr-oxide can provide a passive layer and control the dissolution of vanadium. In order to clarify the difference in corrosion behaviour between the V–Cr and V–Mn phases, which may be solid solutions, each V-rich phase with the composition shown in Table 1 was prepared by arc melting and then potentiodynamic polarization curves were measured. The potentiodynamic curve for the V–Mn phase was more active, see Fig. 7. The corrosion potential was approximately 0.2 V more negative than that for the V–Mn phase, and the anodic current in the passive region was higher by four orders of magnitude.

Table 4
EDX analysis (at.%) of $Zr_{1-x}Ti_xV_{0.6}Ni_{1.2}Mn_{0.2}$ alloys

		$x = 0.0$	$x = 0.25$	$x = 0.50$	$x = 0.75$
A (matrix, C14)	Zr	28	21	17	8
	Ti		7	14	20
	V	27	24	21	25
	Ni	38	41	41	39
	Mn	7	7	7	8
B (Zr–Ti–Ni)	Zr	40	27	12	5
	Ti		13	27	33
	V	2	3	6	8
	Ni	57	55	53	51
	Mn	1	1	2	3
C (V-rich)	Zr		<1	<1	<1
	Ti		1	4	8
	V		81	77	68
	Ni		6	7	12
	Mn		12	12	12

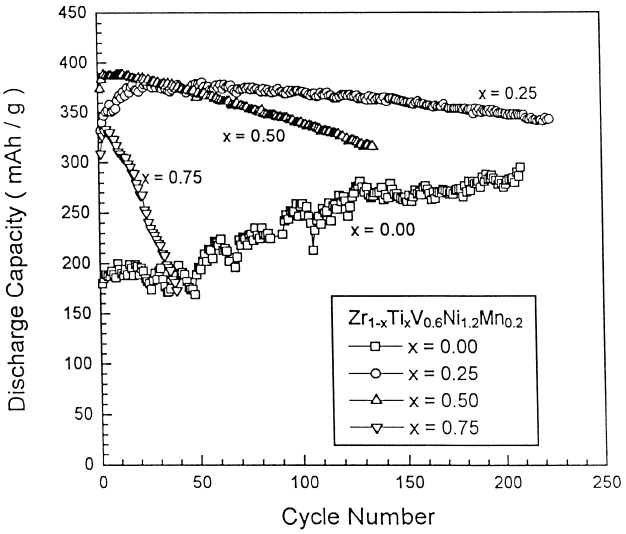

Fig. 12. Cycle performance of $Zr_{1-x}Ti_xV_{0.6}Ni_{1.2}Mn_{0.2}$ ($x = 0.0$, 0.25, 0.50, 0.75) alloy electrodes.

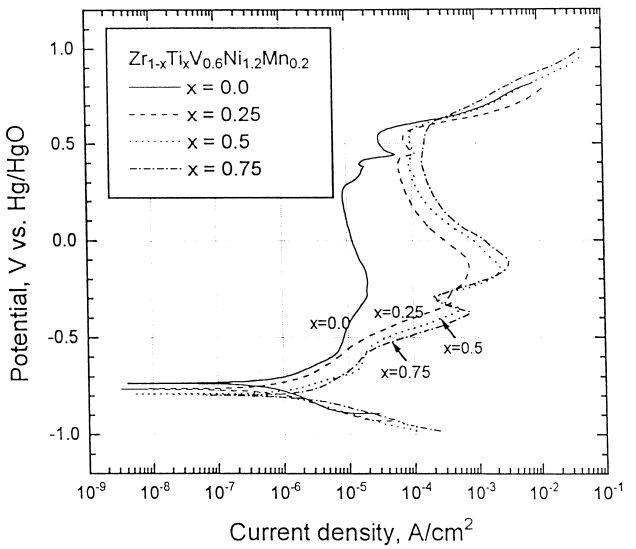

Fig. 13. Potentiodynamic polarization behaviour of $Zr_{1-x}Ti_xV_{0.6}Ni_{1.2}Mn_{0.2}$ ($x = 0.0$, 0.25, 0.50, 0.75) alloy ingots.

3.2. Effect of Zr:Ti ratio in $Zr_{1-x}Ti_xV_{0.6}Ni_{1.2}Mn_{0.2}$ ($x = 0$, 0.25, 0.5, 0.75) alloy system

Optimizing the Zr:Ti ratio to improve the cycle life of the $Zr_{1-x}Ti_xV_{0.6}Ni_{1.2}Mn_{0.2}$ alloy while maintaining its high discharge capacity was investigated. From the V–Ti binary phase diagram, it is known that V also can form a solid solution with Ti. Thus, it is expected that the amount of V–Mn phase, shown to be susceptible to vanadium dissolution in the electrolyte, can be decreased by lowering the Ti content in the alloy.

3.2.1. Alloy microstructure

The main phase of each alloy was identified, by means of XRD analysis, as the C14 Laves phase. Electron micrographs of the $Zr_{1-x}Ti_xV_{0.6}Ni_{1.2}Mn_{0.2}$ alloy system are presented in Figs. 8–11. The chemical composition of each region labelled in the micrographs is summarized in Table 4. The measured volume percent of the V–Mn phase was 0, 3, 9 and 11% for $x = 0.0$, 0.25, 0.5 and 0.75, respectively. Hence, the amount of the V-rich phase increases with increasing Ti content in the alloy.

3.2.2. Cycle life and corrosion behaviour of the alloys

The results of cycle tests of the $Zr_{1-x}Ti_xV_{0.6}Ni_{1.2}Mn_{0.2}$ alloys with $x = 0$, 0.25, 0.5, and 0.75 are given in Fig. 12. The cycle life increases with decreasing Ti content in the alloy; the life improved when the Ti content decreased from $x = 0.5$ to 0.25 without noticeable decrease in discharge capacity.

The vanadium dissolution rate of each alloy electrode is listed in Table 5. The increase in dissolution rate with Ti content is proportional to the rate of capacity loss during charge–discharge cycling. The potentiodynamic behaviour of each alloy ingot is shown in Fig. 13. The corrosion potential and the current for each alloy, which were obtained from potentiodynamic curves, are also listed in Table 5. The corrosion current increases with increasing Ti content in the alloy. The stability of the surface oxide of the alloy, characterized by potentiodynamic curves in the region above -0.5 V (vs. Hg/HgO), decreases with increasing Ti content in the alloy.

In summary, the results show that the corrosion resistance of the alloy increases with decreasing Ti content in the alloy, and this results in an increase in cycle life. The influence of Ti content on the corrosion behaviour can be attributed to two possible causes. First, the segregated V-rich phase in the alloy, which is more corrosive in the alkaline solution than the matrix phase (C14 Laves phase), may be less plentiful when less Ti is present. Second, the corrosion resistance of the matrix phase between the alloys may be different for each alloy. The analysis of the chemical composition of the alloy matrix (Table 4) shows

Table 5
Corrosion potential (E_{corr}) and current (I_{corr}), percent of capacity decrease and V-dissolution per cycle of $Zr_{1-x}Ti_xV_{0.6}Ni_{1.2}Mn_{0.2}$ alloys

$x =$	E_{corr} (V vs. Hg/HgO)	I_{corr} (μA cm^{-2})	Capacity decrease per cycle (%) $\times 10^2$	V-dissolution per cycle (%) $\times 10^2$
0.0	−0.734	0.59	–	–
0.25	−0.764	0.64	5.0	6.5
0.5	−0.792	1.20	12.8	13.8
0.75	−0.797	2.56	90.0	75.0

that there is a noticeable difference in the composition among alloys with different Zr:Ti ratios. This difference in composition increases with increasing Zr content. Cycle tests (Fig. 12) reveal that more cycles are required to activate the alloys to reach a saturated discharge capacity when the Zr:Ti ratio is increased. It is known that the activation rate is influenced by the porosity of the surface oxide present in the alloy powder, which may be increased by dissolution of vanadium from the alloy. Therefore, it is suggested that the corrosion resistance of the matrix Laves phase can be improved by finding an optimum Zr:Ti ratio for the alloy. If Ti is absent, then the Zr-based alloys yield lower capacity which gradually increases with cycling. When too much Ti is added ($x > 0.5$), the cycle performance displays a very fast activation and higher capacities, but the capacity decays quickly within 100 cycles for $x = 0.5$ and 50 cycles for $x = 0.75$.

4. Conclusions

The relationship between the cycle life and the corrosion behaviour of hydrogen-storage alloy electrodes has been investigated in terms of active–passive kinetics according to the metallurgical microstructure and composition. Substituting a fraction of the nickel in the original alloy with Cr increases the cycle life of the original $Zr_{0.5}Ti_{0.5}V_{0.6}Ni_{1.4}$ alloy due to the formation of a V–Cr solid solution which inhibits vanadium dissolution into alkaline electroyte. Substituting Ni with Mn causes an increase in the discharge capacity, but the cycle life is shortened due to the formation of a V–Mn phase which is corrosive in alkaline electrolyte.

The Zr:Ti ratio in $Zr_{1-x}Ti_xV_{0.6}Ni_{1.2}Mn_{0.2}$ has been varied to extend the cycle life of the Mn-substituted alloy. An optimum composition is found to be $x = 0.25$. The improvement of cycle life by increasing the Zr content in the alloy is attributed to an improvement in the corrosion resistance of the alloy due to a decrease in formation of the corrosive V–Mn phase and also a possible increase in the corrosion resistance of the Laves phase matrix.

References

[1] J.J.G. Willems, K.H.J. Buschow, J. Less Common Met. 129 (1987) 13–30.
[2] S. Ovshinsky, M. Fetcenko, J. Ross, Science 260 (1993) 176–181.
[3] S. Mukerjee, J. McBreen, J.J. Reilly, J.R. Johnson, G.D. Adzic, M.R. Marrero, 192nd Meeting of the Electrochemical Society, Paris, vol. 97-2, Abs. #290 (1997).
[4] H. Miyamura, T. Sakai, N. Kuriyama, K. Oguro, A. Kato, H. Ishikawa, in: D.A. Corrigan, S. Srinivasan (Eds.), Proceedings of the Symposium on Hydrogen Storage Materials, Batteries and Electrochemistry, The Electrochemical Society, (1992) 179–198.
[5] S. Venkatesan, B. Reichman, M.A. Fetcenko, U.S. Patent 4,827,586 (1988).
[6] T. Lyman (Ed.), Phase Diagrams of Binary Alloy Systems, Metals Handbook, 8th edn., vol. 8, 1973, p. 337.
[7] B.V. Ratnakumar, C. Witham, B. Fultz, G. Halpert, J. Electrochem. Soc. 141 (1994) L89–L91.